# Frequency estimation precision in Doppler optical coherence tomography using the Cramer-Rao lower bound

**Siavash Yazdanfar, Changhuei Yang, Marinko V. Sarunic, Joseph A. Izatt**

*Department of Biomedical Engineering*
*Duke University, Durham, NC 27708*

**Abstract:** Doppler optical coherence tomography (DOCT) is a technique for simultaneous cross-sectional imaging of tissue structure and blood flow. We derive the fundamental uncertainty limits on frequency estimation precision in DOCT using the Cramer-Rao lower bound in the case of additive (e.g., thermal, shot) noise. Experimental results from a mirror and a scattering phantom are used to verify the theoretical limits. Our results demonstrate that the stochastic nature of frequency noise influences the precision of flow imaging, and that the noise model must be selected judiciously in order to estimate the frequency precision.



**OCIS codes**: (170.4500) Optical coherence tomography; (170.3340) Laser Doppler velocimetry; (120.5050) Phase measurement

## References and links

1. Z. P. Chen, T. E. Milner, D. Dave and J. S. Nelson, "Optical Doppler tomographic imaging of fluid flow velocity in highly scattering media," Opt. Lett. **22**, 64-66 (1997).
2. J. A. Izatt, M. D. Kulkarni, S. Yazdanfar, J. K. Barton and A. J. Welch, "*In vivo* bidirectional color Doppler flow imaging of picoliter blood volumes using optical coherence tomography," Opt. Lett. **22**, 1439-1441 (1997).
3. D. Huang, E. A. Swanson, C. P. Lin, J. S. Schuman, W. G. Stinson, W. Chang, M. R. Hee, T. Flotte, K. Gregory, C. A. Puliafito and J. G. Fujimoto, "Optical coherence tomography," Science **254**, 1178-1181 (1991).
4. S. Yazdanfar, A. M. Rollins and J. A. Izatt, "Imaging and velocimetry of the human retinal circulation using color Doppler optical coherence tomography," Opt. Lett. **25**, 1448-1450 (2000).
5. S. Yazdanfar, A. M. Rollins and J. A. Izatt, "*In vivo* imaging of human retinal flow dynamics by color Doppler optical coherence tomography," Arch. Ophthalmol. **121**, 235-239 (2003).
6. R. A. Leitgeb, L. Schmetterer, W. Drexler, A. F. Fercher, R. J. Zawadzki and T. Bajraszewski, "Real-time assessment of retinal blood flow with ultrafast acquisition by color Doppler Fourier domain optical coherence tomography," Opt. Express **11**, 3116-3121 (2003). http://www.opticsexpress.org/abstract.cfm?URI=OPEX-11-23-3116
7. B. R. White, M. C. Pierce, N. Nassif, B. Cense, B. H. Park, G. J. Tearney, B. E. Bouma, T. C. Chen and J. F. de Boer, "*In vivo* dynamic human retinal blood flow imaging using ultra-high-speed spectral domain optical Doppler tomography," Opt. Express **11**, 3490-3497 (2003). http://www.opticsexpress.org/abstract.cfm?URI=OPEX-11-25-3490
8. Y. Zhao, Z. P. Chen, C. Saxer, S. Xiang, J. F. de Boer and J. S. Nelson, "Phase-resolved optical coherence tomography and optical Doppler tomography for imaging blood flow in human skin with fast scanning speed and high velocity sensitivity," Opt. Lett. **25**, 114-116 (2000).
9. D. Piao, L. L. Otis, N. K. Dutta and Q. Zhu, "Quantitative assessment of flow velocity-estimation algorithms for optical Doppler tomography imaging," Appl. Opt. **41**, 6118-6127 (2002).
10. V. X. D. Yang, M. L. Gordon, S.-J. Tang, N. E. Marcon, G. Gardiner, B. Qi, S. Bisland, E. Seng-Yue, S. Lo, J. Pekar, B. C. Wilson and I. A. Vitkin, "High speed, wide velocity dynamic range Doppler optical coherence tomography (Part III): *in vivo* endoscopic imaging of blood flow in the rat and human gastrointestinal tracts," Opt. Express **11**, 2416-2424 (2003). http://www.opticsexpress.org/abstract.cfm?URI=OPEX-11-19-2416

#5961 - $15.00 US Received 3 December 2004; revised 29 December 2004; accepted 5 January 2005

11. Y. Imai and K. Tanaka, "Direct velocity sensing of flow distribution based on low-coherence interferometry," J. Opt. Soc. Am. A **16**, 2007-2012 (1999).
12. S. Yazdanfar, M. D. Kulkarni and J. A. Izatt, "High resolution imaging of *in vivo* cardiac dynamics using color Doppler optical coherence tomography," Opt. Express **1**, 424-431 (1997). http://www.opticsexpress.org/abstract.cfm?URI=OPEX-1-13-424
13. S. Yazdanfar and J. A. Izatt, "Self-referenced Doppler optical coherence tomography," Opt. Lett. **27**, 2085-2087 (2002).
14. H. L. Van Trees, *Detection, estimation, and modulation theory, Pt. 1* (John Wiley & Sons, New York, 1968).
15. L. L. Scharf, *Statistical signal processing: Detection, estimation, and time series analysis* (Addison-Wesley Publishing Co., Reading, MA, 1991).
16. J. W. Goodman, *Statistical Optics* (John Wiley & Sons, Inc., Hoboken, NJ, 1985).
17. M. Bashkansky and J. Reintjes, "Statistics and reduction of speckle in optical coherence tomography," Opt. Lett. **25**, 545-547 (2000).
18. M. D. Kulkarni, T. G. van Leeuwen, S. Yazdanfar and J. A. Izatt, "Velocity estimation accuracy and frame rate limitations in color Doppler optical coherence tomography," Opt. Lett. **23**, 1057-1059 (1998).
19. A. M. Rollins, S. Yazdanfar, J. K. Barton and J. A. Izatt, "Real-time *in vivo* color Doppler optical coherence tomography," J. Biomed. Opt. **7**, 123-129 (2002).
20. V. X. D. Yang, M. L. Gordon, B. Qi, J. Pekar, S. Lo, E. Seng-Yue, A. Mok, B. C. Wilson and I. A. Vitkin, "High speed, wide velocity dynamic range Doppler optical coherence tomography (Part I): System design, signal processing, and performance," Opt. Express **11**, 794-809 (2003). http://www.opticsexpress.org/abstract.cfm?URI=OPEX-11-7-794
21. D. A. Boas, K. K. Bizheva and A. M. Siegel, "Using dynamic low-coherence interferometry to image Brownian motion within highly scattering media," Opt. Lett. **23**, 319-321 (1998).

## 1. Introduction

Doppler optical coherence tomography (DOCT) [1,2] enables the simultaneous imaging of structure and blood flow with high spatial (~10 μm) and velocity (~10-100 μm/s) resolution in the microvasculature of living tissues. Structural imaging is performed by monitoring the amplitude of interference between light reflected from a sample and a reference reflector [3]. The phase of the interferometric data contains information regarding the sample and reference Doppler frequencies [2], and has been used for depth-resolved blood flow measurement in human retina [4-7], skin [8,9] and gastrointestinal tract [10].

DOCT operates as a heterodyne optical receiver as shown schematically in Fig. 1. The component of the heterodyne detector current resulting from interference between light returning from the reference mirror and a given scatterer in the sample is given by [2]

$$s(t) = A(t)\cos[2\pi(f_r - f_s)t + \beta(t)], \tag{1}$$

where $A(t)$ is the time-dependent amplitude of the interferogram used in conventional OCT images, $f_r$ is the fixed Doppler frequency induced by the reference arm scanning, $f_s$ is the Doppler frequency owing to motion (e.g., flow) in the sample arm, and the phase term $\beta(t)$ is a term describing the axial position of the scatterer and phase drifts in the interferometer incurred over the observation time. It is often assumed that the contribution of noise to $\beta(t)$ is minimal and invariant over the observation time, although this assumption may be invalid during measurement of low velocities.

Quantitative analysis of the phase component arising from the sample arm determines the axial velocity component of flowing scatterers. Analytical techniques for measuring the transverse velocity component have also been described [11]. The DOCT interferometric signal demodulated at the reference arm Doppler frequency is given by

$$s(t) = A(t)\cos[2\pi f_s t + \beta(t)], \;\; 0 \le t \le t_0 \tag{2}$$

#5961 - $15.00 US Received 3 December 2004; revised 29 December 2004; accepted 5 January 2005

where $t_0$ is the observation time used to estimate flow, and the constant relative phase accrued by the demodulation process is ignored. This single frequency model is valid and widely used in DOCT [1,2].

Since the microcirculation is composed of small blood vessels with low volumetric flow rates, the ability of DOCT to detect blood flow in capillaries is determined by the spatial and velocity resolutions of the imaging system. Whereas the coherence length of the light source and the beam spot size in the sample determine the axial and transverse spatial resolutions [3], respectively, the smallest resolvable Doppler frequency ( $f_s^{\min}$ ) determines the velocity resolution. As a first approximation, $f_s^{\min}$ has been estimated as being inversely proportional to the observation time [2,12]:

$$f_s^{\min} = \frac{1}{t_0} \tag{3}$$

This quantity, also known as the Fourier limit, can be interpreted as the lowest frequency harmonic captured during the observation time. In practice, however, a full period of this harmonic need not be collected for accurate frequency estimation. If the local image signal-to-noise ratio (SNR) is sufficiently high (e.g., resulting from a bright reflection from the sample) the frequency precision may surpass the Fourier limit. This effect has been confirmed experimentally in previous DOCT measurements [13].

It is well known in remote sensing technologies such as radar and sonar that the ability to estimate a frequency depends upon both the statistical properties of noise at the receiver and the estimator used to determine the frequency [14]. The Cramer-Rao lower bound (CRLB) is used to determine the lowest bound on the performance of an unbiased estimator. Here we derive, via the CRLB, the fundamental uncertainty limits on frequency estimation precision in DOCT. The limits are verified with experiments using a highly scattering phantom.

## 2. Theory

Frequency precision is determined by the quality of the estimate, given by its variance. The variance of an unbiased estimate $\hat{\alpha}$ of a parameter $\alpha$ is given by the CRLB [14,15]:

$$Var\left[\hat{\alpha}(\vec{R}) - \alpha\right] \geq \left( E\left\{ \left[ \frac{\partial \ln p(\vec{R} \mid \alpha)}{\partial \alpha} \right]^2 \right\} \right)^{-1} \tag{4}$$

where $E\{\cdot\}$ denotes the expected value and $p(\vec{R} \mid \alpha)$ is the likelihood of having observed the data vector $\vec{R}$ given $\alpha$. The receiver signal $r(t)$ can be modeled as the summation of an ideal signal $s(t,\alpha)$ and noise $n(t)$:

$$r(t) = s(t,\alpha) + n(t) \tag{5}$$

In the case that $n(t)$ is Gaussian and purely additive (e.g., thermal or shot noise), the variance of an estimate is given by [14]

$$\sigma_{\hat{\alpha}}^2 \geq \left( \frac{1}{N_0} \int_0^{t_0} \left[ \frac{\partial s(t,\alpha)}{\partial \alpha} \right]^2 dt \right)^{-1} \tag{6}$$

where $N_0$ is the noise energy spectral density. The maximum-likelihood estimator satisfies the equality condition in Eq. (6). For the signal of Eq. (2), assuming a uniform signal amplitude distribution, the variance of the estimate $\hat{f}$ of the sample arm Doppler frequency is

#5961 - $15.00 US Received 3 December 2004; revised 29 December 2004; accepted 5 January 2005

$$\sigma_{\hat{f}}^2 \geq \left( \frac{2\pi^2}{3} \frac{A^2}{N_0} t_0^2 \right)^{-1} \tag{7}$$

The minimum resolvable Doppler frequency is equal to the standard deviation of the estimator, $\sigma_{\hat{f}}$, evaluated at the equality in Eq. (7). Since $SNR \sim A^2/N_0$, the frequency precision improves with increasing signal-to-noise ratio

$$f_s^{\min} \approx \sigma \propto \frac{1}{t_0 \sqrt{SNR}} \tag{8}$$

The additive-noise-only model is incomplete when imaging a turbid sample. In this case, the sampling volume at each axial position in the image contains several scatterers, each of which contributes a random phase term $\beta(t)$. If this term is uniformly distributed between 0 and 2π, the probability density function of the detected complex signal is the well-known circular Gaussian distribution present in speckle statistics [16,17], and can be interpreted as multiplicative noise. The contribution of speckle to frequency estimation has previously [18] been described by an empirical constant, related to the width of the frequency spectrum, multiplied by the Fourier limit.

## 3. Methods

In order to experimentally verify the relationship in Eq. (7), we measured the standard deviation of the frequency estimate as a function of image signal-to-noise ratio. A schematic of the DOCT system is shown in Fig. 1. A superluminescent diode with a 24.5 nm bandwidth centered at $\lambda_0$ = 826 nm (resulting in a free space theoretical axial resolution of 12.3 μm) illuminated the interferometer. Reference arm scanning was performed with a retroreflecting mirror mounted on a galvanometer scanning linearly at 33.8 mm/s (~7 lines/s). The sample consisted of either a stationary mirror or an intravenous fat emulsion (Liposyn, 0.8% solid) commonly used as a scattering phantom. The sample arm light was focused to a spot size of ~9 μm. Using a nominally stationary sample ensured that any residual sample arm Doppler frequency resulted primarily from receiver noise, although mechanical vibrations may also contribute to noise.

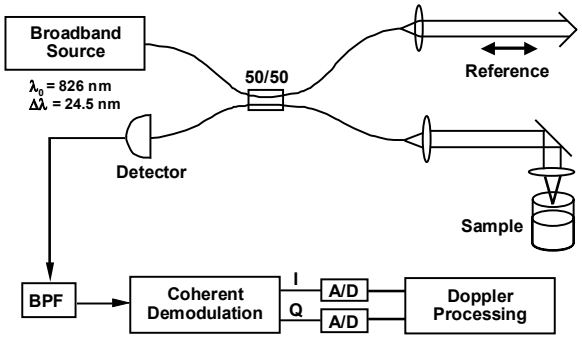


Fig. 1. Fiber-optic, time-domain Michelson interferometer used to measure the frequency precision of Doppler OCT. BPF, band-pass filter; A/D, analog-to-digital converter; I, Q, in-phase and quadrature signal components after demodulation.

Interference between light backreflected from the reference and sample arms was detected with a silicon photodetector. The resulting output signal was demodulated at the Doppler frequency ($f_r = 81.8$ kHz) induced by the reference arm motion. The demodulated

#5961 - $15.00 US Received 3 December 2004; revised 29 December 2004; accepted 5 January 2005

quadrature components were digitized for off-line Doppler processing using an autocorrelation algorithm [13,19]. The sample arm Doppler frequency $f_s = \phi(\tau)/2\pi\tau$ was determined by the phase $\phi(\tau)$ of the autocorrelation of axial scans

$$R(\tau) = \left|R(\tau)\right| \exp[-i\phi(\tau)] \equiv \left\langle s^*(t)s(t+\tau)\right\rangle \tag{9}$$

evaluated at a single delay (lag) $\tau = \tau_{PIXEL}$, the pixel sampling time. Angular brackets denote ensemble averaging, implemented by a second-order low-pass Bessel filter. The observation time $t_0$ used to calculate the theoretical frequency precision corresponds to the response time of the filter. For each image, the frequency precision was measured by calculating the standard deviation of $f_s$ at each axial location for 100 line-scans. The local SNR was measured by dividing the average signal at each axial pixel by the standard deviation of the image noise in a region of interest that contained no signal. The procedure for calculating the frequency precision and SNR is summarized in Fig. 2.

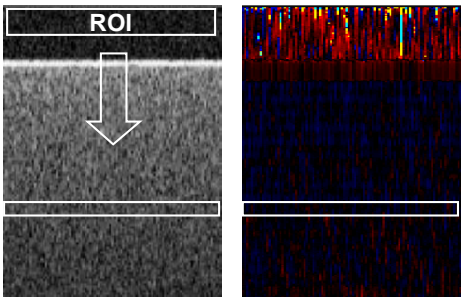


Fig. 2. Algorithm for calculating frequency precision and signal-to-noise ratio (SNR). The OCT reflectance image of Liposyn is shown on the left, with the arrow indicating the direction of the incident beam. The standard deviation of the noise is calculated in the region of interest (ROI) located outside of the sample. At each axial position, the average signal value across 100 scans is measured and divided by the noise to measure local SNR. At the same depth, the variance of the Doppler frequency (right) is measured and compared to the theoretical frequency precision.

## 4. Results and discussion

The frequency precision was measured using a stationary mirror in the sample arm. Since the signal arises from a single reflection, this case ensures that predominantly additive receiver noise dominates. The frequency precision as a function of SNR for the additive noise condition is plotted in Fig. 3(a) in comparison to the Fourier limit {Eq. (3)} and CRLB {Eq. (7)}. For all SNR values, the measured frequency precision exceeded the Fourier limit by as much as an order of magnitude, but consistently satisfied the CRLB. The measured precision indicates an inverse dependence on SNR, as predicted by the CRLB. At the highest SNR values, the precision appears to plateau, suggesting a systematic noise source that is not accounted for. Nevertheless, Eq. (7) appears to be a more accurate measure of frequency precision in DOCT in the case of additive noise.

Next, the frequency precision was measured from a sample consisting of scattering lipid particles. In contrast to the previous experiment that contained a single specular reflection, the sampling volume at each axial position in the image contained several scatterers, each of which contributes a scattered phase term. The stochastic interference of these phase terms at the detector results in multiplicative noise in the form of speckle. As shown in Fig. 3(b), the standard deviation of the frequency estimate relative to the theoretical limits is much greater in the scattering medium than in the specular reflection. At no point does the experimental

#5961 - $15.00 US Received 3 December 2004; revised 29 December 2004; accepted 5 January 2005

data exceed the Fourier limit, although it should be noted that the SNRs were considerably lower than the previous experiment. This experiment suggests that at low SNR the Fourier limit is a useful rule-of-thumb estimate of the frequency precision, although it is not strictly accurate and fails to account for the SNR-dependence of the estimate. The inverse dependence of DOCT frequency precision on image SNR has also been observed by others [20]. Additionally, these results indicate that the additive model, combined with the assumption of constant signal amplitude, fail to account for the speckle noise in a turbid medium. The CRLB may also be derived using relevant models that more closely approximate the signal in the presence of multiplicative noise.

In a turbid sample, another potential source of uncertainty in measurement of the Doppler frequency is due to Brownian motion of scatterering particles. In an aqueous solution, this Brownian motion component results in a frequency broadening of [21]

$$\Omega = 16\left(\pi / \lambda_0\right)^2 D_T \quad \text{[rad/s]} \tag{10}$$

where $D_T = k_B T / 3\pi\eta a$ is the translational diffusion coefficient, $k_B$ is Boltzmann's constant, $T$ is the temperature, $\eta$ is the viscosity of the fluid, and $a$ is the particle diameter. Considering the average size $a \sim 400\,\text{nm}$ of fat particles in Liposyn, resulting in $D_T \sim 1.1\times10^{-8}$ cm$^2$/s, the spectral uncertainty due to Brownian motion is approximately 40 Hz. Since frequency resolutions in DOCT on the order of 1 Hz have been demonstrated [13], the Brownian effect can considerably affect Doppler frequency estimates in high frequency-resolution DOCT measurements, such as those for which the processing is performed across sequential scans [6-8,13,20]. However, *in vivo* applications are typically less sensitive to this error source, since the dominant scatterer in blood vessels is the red blood cell ($a \sim 6-8\,\mu\text{m}$) resulting in $\Omega/2\pi \sim 2-3$ Hz. Finally, since the thermal noise in two distinct detector channels is statistically uncorrelated, we anticipate that the CRLB will hold even in the case of phase-referenced interferometric detection of DOCT [13].

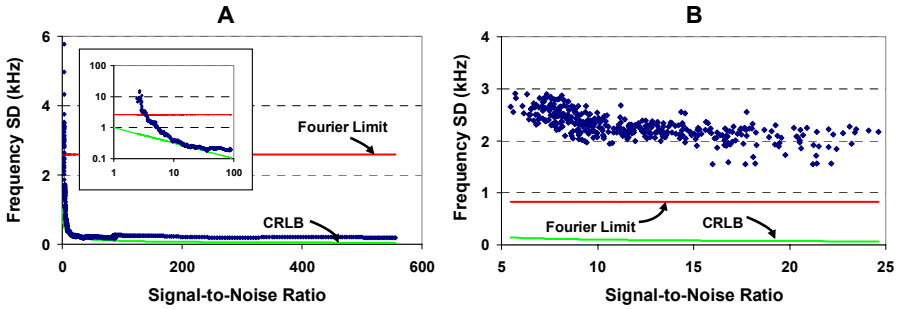


Fig. 3. Experimental and theoretical frequency standard deviation (SD) versus SNR for A) additive noise only and B) both additive and multiplicative (speckle) noise. The observation time was different for the two experiments, resulting in different theoretical limits. The inset of A), magnifying lower SNR values on a log-log scale, suggests that the autocorrelation algorithm used to estimate frequency is a maximum likelihood estimator. CRLB, Cramer-Rao lower bound based on the additive model of Eqs. (2) and (5).

In conclusion, the Cramer-Rao lower bound was applied to estimation of frequency precision in DOCT. It was shown that the stochastic nature of frequency noise determines the ability to accurately estimate velocity for blood flow imaging. In the absence of multiplicative noise, the CRLB consistently exceeded the Fourier limit. Experiments in a scattering phantom verified that the variance of the frequency estimate decreases monotonically with the local signal-to-noise ratio. The CRLB can be used to determine the

#5961 - $15.00 US Received 3 December 2004; revised 29 December 2004; accepted 5 January 2005

quality of algorithms to estimate the Doppler frequency in DOCT. This limit should hold for spectral domain OCT [6,7] as well as the conventional time-domain OCT methods shown here.

**Acknowledgments**

This study was supported by National Institutes of Health grant EY-13015. We gratefully acknowledge fruitful discussions with Jeff Krolik at Duke University, Bill Walker at the University of Virginia, and Jason Connor at Carnegie Mellon University. S. Yazdanfar is currently with the Massachusetts Institute of Technology, Cambridge, MA. C. Yang is currently with the California Institute of Technology, Pasadena, CA.

#5961 - $15.00 US Received 3 December 2004; revised 29 December 2004; accepted 5 January 2005